

Tunneling spectrum of a pinned vortex with a robust Majorana state

R. S. Akzyanov,^{1,2,3} A. V. Rozhkov,^{1,2,4} A. L. Rakhmanov,^{1,2,3,4} and Franco Nori^{4,5}

¹*Moscow Institute for Physics and Technology (State University), 141700 Moscow Region, Russia*

²*Institute for Theoretical and Applied Electrodynamics, Russian Academy of Sciences, 125412 Moscow, Russia*

³*All-Russia Research Institute of Automatics, 22 Sushchevskaya, Moscow 127055, Russia*

⁴*CEMS, RIKEN, Saitama, 351-0198, Japan*

⁵*Department of Physics, University of Michigan, Ann Arbor, Michigan 48109-1040, USA*

(Received 26 August 2013; revised manuscript received 7 November 2013; published 11 February 2014)

We study a heterostructure which consists of a topological insulator and a superconductor with a hole. The hole pins a vortex. The system supports a robust Majorana fermion state bound to the vortex core. We investigate the possibility of using scanning tunneling spectroscopy (i) to detect the Majorana fermion in the proposed setup and (ii) to study excited states bound to the vortex core. The Majorana fermion manifests itself as a magnetic-field-dependent zero-bias anomaly of the tunneling conductance. Optimal parameters for detecting Majorana fermions have been obtained. In the optimal regime, the Majorana fermion is separated from the excited states by a substantial gap. The number of zero-energy states equals the number of flux quanta in the hole; thus, the strength of the zero-bias anomaly depends on the magnetic field. The lowest energy excitations bound to the core are also studied. The excited states spectrum differs from the spectrum of a typical Abrikosov vortex, providing additional indirect confirmation of the Majorana state observation.

DOI: [10.1103/PhysRevB.89.085409](https://doi.org/10.1103/PhysRevB.89.085409)

PACS number(s): 71.10.Pm, 03.67.Lx, 74.45.+c

I. INTRODUCTION

In 1937 Majorana derived [1] an alternative representation of the Dirac equation for particles with spin 1/2. In this representation the Dirac equation has an additional solution, the so-called Majorana fermion. This unusual particle is equal to its antiparticle, that is, for the Majorana fermion,

$$\gamma = \gamma^\dagger. \quad (1)$$

This is impossible for the usual Dirac fermions. Among the elementary particles, the neutrino is a candidate for the Majorana fermion, but this is not firmly established yet. Several setups [2–15] have been theoretically proposed for observing Majorana fermions in condensed matter systems, e.g., excitations in the quantum Hall effect, in topological superconductors of $(p_x + ip_y)$ type, wires with strong spin-orbit interaction, etc. The observation of Majorana fermions is of interest not only for fundamental physics but also for potential applications. Majorana fermions are expected to exhibit non-Abelian statistics and could be used to realize quantum gates that are topologically protected from local sources of decoherence [16]. Recent experiments [17,18] hinted at the existence of a Majorana fermion in nanowires coupled to superconductors and in hybrid superconductor-topological insulator devices. However, the problem is still open, and no smoking-gun evidence has surfaced.

A. Previous results

The interface between a topological insulator and a superconductor is a candidate system for the possible realization of Majorana fermions [11,12,19–21]. Such an interface has been fabricated in experiments [18,22–25]. Electrons on the surface of topological insulators are described by the two-dimensional (2D) massless Dirac equation, where the electron and hole excitations lie on a Dirac cone $\varepsilon_{\mathbf{k}} = v_F|\mathbf{k}|$, and the Dirac point of this cone is located at the Fermi level [26]. The contact

between the topological insulator and the superconductor generates, through the proximity effect, a finite mass to these Dirac fermions. In the presence of an external magnetic field, the mass term acquires a nontrivial complex phase. Several theoretical proposals for the realization of Majorana fermions are based on this setup [11,12,19–21].

In this paper we discuss the system presented in Ref. [19] (see Fig. 1). It consists of three layers: the topological insulator at the bottom, a sufficiently thick layer of an s -wave superconductor on top, and between them a thin buffer insulating layer, which controls the electron tunneling between the topological insulator and the superconductor. The system is placed in a weak magnetic field to create a vortex in the superconductor and, consequently, a 2D vortex in the 2D superconducting state induced on the surface of the topological insulator. The core of the 2D vortex hosts the Majorana fermion state [27].

In general, a setup of this type has an obvious deficiency, which hampers the detection of the Majorana fermion state: the minigap separating the Majorana fermion and the so-called Caroli-de Gennes-Matricon (CdGM) levels in the core of the Abrikosov vortex [28] is too small (about 10^{-2} K). To detect the Majorana fermion, both the temperature and the experimental energy resolution must be smaller than the minigap, thus, the smallness of the minigap imposes very stringent requirements on experiments.

Fortunately, it is known that, when an Abrikosov vortex is pinned by a columnar defect, the minigap increases when increasing the defect radius [29]. This happens because the lowest CdGM states are destroyed by the defect. Consequently, the minigap, as a function of the defect radius R , saturates when $R \sim \xi$, where ξ is the superconducting coherence length. In such a regime, virtually all CdGM states are destroyed. Based on this idea, it was proposed [19] to pin the Abrikosov vortex on a hollow cylindrical channel in the superconducting layer (see Fig. 1). The purpose of this “hole” is twofold: It rids the system of a large set of parasitic CdGM excitations,

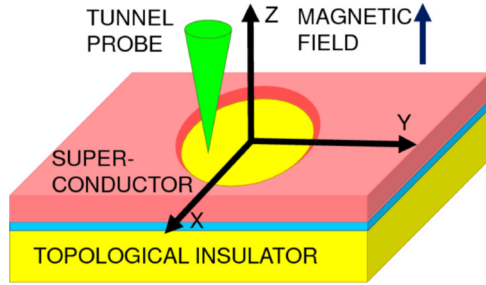


FIG. 1. (Color online) Proposed experimental setup for detecting a Majorana fermion. A layer of superconducting material (pink) is separated from a slab of topological insulator (yellow) by a thin insulating layer (blue). The external magnetic field is perpendicular to the interface. A cylindrical hole in the superconductor serves as a pinning center for a vortex. The tunneling conductance between the tunneling probe (green) and the open fraction of the topological insulator surface is used to investigate the low-lying single-electron states bound to the vortex core.

and also allows access to the surface of the topological insulator.

As for CdGM states inside the 2D vortex core, it was demonstrated [12,19] that, if the chemical potential of the 2D Dirac electrons lies sufficiently close to the Dirac point, the corresponding minigap is quite large, making the Majorana state “robust” (related ideas for different physical systems have been discussed in Ref. [13]).

B. Our results

The above arguments, however, are purely theoretical. To demonstrate that the proposed system does indeed host a Majorana fermion, a reliable experimental proof is required. The purpose of this paper is to investigate the usefulness of scanning tunneling spectroscopy (STS) as a tool to diagnose the presence of the Majorana fermion in the setup of Fig. 1.

To address this question we discuss two related problems: First, what STS features are associated with the presence of the Majorana fermion in our setup; second, what are the system parameters which optimize the observation of these features. Below we will demonstrate that, even at not-too-low temperatures, the tunneling spectrum can be used to identify the Majorana state in the proposed system.

The remainder of the paper is organized as follows. In Sec. II the Bogolyubov-de Gennes equations are derived. The zero-energy solutions (zero modes) of these equations are discussed in Sec. III. The tunneling spectrum at arbitrary energy is discussed in Sec. IV. The results are discussed in Sec. V.

II. BOGOLYUBOV-DE GENNES EQUATIONS

In this section we derive the differential equations for the wave functions of the single-electron eigenstates bound to the vortex core. The proximity effect in 2D materials has been studied in several papers [30–32]. Our derivation generalizes the procedure of Refs. [12,19] to account for an arbitrary number of vortices trapped in the hole. The presentation below

is quite sketchy. For extra details the reader should consult Refs. [12,19].

A. Microscopic model

The Hamiltonian of the system can be written as [12]

$$H = H_{\text{TI}} + H_{\text{SC}} + T + T^\dagger, \quad (2)$$

where $H_{\text{TI}}, H_{\text{SC}}$ are related to the topological insulator (TI) and the superconductor (SC), respectively. The term T describes the tunneling from the topological insulator to the superconductor, and T^\dagger accounts for the tunneling from the superconductor to the topological insulator. The corresponding Bogolyubov-de Gennes equations [28] are ($\hbar = 1$)

$$H_{\text{TI}}\psi_{\text{TI}} + T^\dagger\psi_{\text{SC}} = \omega\psi_{\text{TI}}, \quad (3)$$

$$H_{\text{SC}}\psi_{\text{SC}} + T\psi_{\text{TI}} = \omega\psi_{\text{SC}}. \quad (4)$$

The terms $H_{\text{TI}}, H_{\text{SC}}$ can be written as 4×4 matrices in the Nambu basis,

$$H_{\text{TI}} = [iv(\sigma \cdot \nabla_r) - U(\mathbf{r})]\tau_z, \quad (5)$$

$$H_{\text{SC}} = -\left(E_F + \frac{\nabla_{\mathbf{R}}^2}{2m}\right)\tau_z + \Delta'(\mathbf{R})\tau_x + \Delta''(\mathbf{R})\tau_y,$$

and $T = \tau_z \mathcal{T}(\mathbf{R} - \mathbf{r})$. In these equations, $\mathbf{R} = (x, y, z)$ is a point in the bulk of the superconductor, $\mathbf{r} = (x, y)$ is a point on the surface of the topological insulator, σ_j, τ_j are the spin and charge Pauli matrices, Δ', Δ'' are the real and imaginary parts of the order parameter in the superconductor, v is the Fermi velocity of the electrons on the surface of the topological insulator, E_F is the Fermi energy in the superconductor, and $U(r)$ is a gate voltage applied to control the Fermi level in the topological insulator [12]. The wave functions $\psi_{\text{TI}, \text{SC}}$ are four-component spinors:

$$\psi_{\text{TI}, \text{SC}} = [u_\uparrow, u_\downarrow, v_\downarrow, -v_\uparrow]^T. \quad (6)$$

In Hamiltonian Eq. (5) the vector potential describing the magnetic field is omitted. This is justified provided that the flux, passing through the area where the subgap wave functions are localized, is smaller than the flux quantum. In the regime we study, the subgap states are localized within distance $r \sim \xi$ from the hole center, consequently, the magnetic field may be neglected when $(\xi/\lambda_L)^2 \ll 1$, where λ_L is the London penetration depth in the superconducting film. Thus, for the type-II superconducting film this condition is well satisfied.

We also neglect the effects of the magnetic field on the superconductor. The magnetic field necessary for a flux quantum to enter the superconductor H_{c1} is much smaller than the thermodynamic field H_c . Thus, the effects of magnetic field on the superconductor are expected to be quite moderate.

It is easy to check that H satisfies the following charge-conjugation symmetry:

$$H = -\tau_y \sigma_y H^* \tau_y \sigma_y. \quad (7)$$

Consequently, for every eigenstate ψ of H with a nonzero eigenenergy $\omega \neq 0$, an eigenstate $\tau_y \sigma_y \psi^*$ with eigenenergy

$-\omega$ is present. This symmetry is very robust: Disorder potential does not destroy this property.

B. Effective Hamiltonian

Following Ref. [12] we exclude ψ_{SC} from Eqs. (3) and (4) to derive

$$(H_{\text{TI}} + \Sigma)\psi_{\text{TI}} = \omega\psi_{\text{TI}}, \quad (8)$$

$$\Sigma = T^\dagger(\omega - H_{\text{SC}})^{-1}T. \quad (9)$$

We are interested in bound states with energies lying within the superconducting energy gap $|\omega| < |\Delta|$. In this case, the self-energy matrix Σ can be calculated quite straightforwardly [12,19]. For low-lying electron states $\mathbf{k} \approx \mathbf{M}$ (here \mathbf{M} is the location of the Dirac cone apex in the topological insulator Brillouin zone), it is equal to

$$\Sigma_{\mathbf{M},\omega} = \lambda \frac{\Delta\tau_x - \omega\tau_0}{\sqrt{|\Delta|^2 - \omega^2}} - \delta U\tau_z, \quad (10)$$

where τ_0 is the 2×2 identity matrix. The parameter λ has the dimension of energy. It characterizes the transparency of the barrier between the topological insulator and the superconductor [12]: when $\lambda \sim E_F$ ($\lambda \ll E_F$), the barrier is transparent (nontransparent). The parameter $\delta U = O(\lambda)$ is the shift of the topological insulator chemical potential due to doping by the superconductor.

Using Eq. (10) we can cast the Bogolyubov-de Gennes Eq. (8) in the form,

$$H_{\text{eff}}\psi_{\text{TI}} = \omega\psi_{\text{TI}}, \quad (11)$$

where the effective Hamiltonian H_{eff} and its parameters are [12]

$$H_{\text{eff}} = [i\tilde{v}(\omega)(\sigma \cdot \nabla_{\mathbf{r}}) - \tilde{U}(\omega)]\tau_z + \tilde{\Delta}'(\omega)\tau_x + \tilde{\Delta}''(\omega)\tau_y, \quad (12)$$

$$\tilde{v}(\omega) = \frac{v\sqrt{|\Delta|^2 - \omega^2}}{\sqrt{|\Delta|^2 - \omega^2 + \lambda}}, \quad (13)$$

$$\tilde{U}(\omega) = \frac{(U + \delta U)\sqrt{|\Delta|^2 - \omega^2}}{\sqrt{|\Delta|^2 - \omega^2 + \lambda}}, \quad (14)$$

$$\tilde{\Delta}(\omega) = \frac{\Delta\lambda}{\sqrt{|\Delta|^2 - \omega^2 + \lambda}}. \quad (15)$$

We see that the effective parameters experience energy-dependent renormalization with respect to the bare quantities.

C. Normalization of the effective wave function

In addition to the effective Hamiltonian, it is desirable to have a normalization condition for the effective wave function ψ_{TI} . The normalization condition in the \mathbf{k} space for the full wave function is

$$\int_{\mathbf{k}} (\psi_{\text{TI}}^{\mathbf{k},\omega})^\dagger \psi_{\text{TI}}^{\mathbf{k},\omega} + \int_{\mathbf{k}k_z} (\psi_{\text{SC}}^{\mathbf{k},k_z,\omega})^\dagger \psi_{\text{SC}}^{\mathbf{k},k_z,\omega} = 1, \quad (16)$$

where the symbol $\int_{\mathbf{k}}$ stands for $\int d^2\mathbf{k}/(2\pi)^2$, and $\int_{\mathbf{k},k_z}$ stands for $\int d^2\mathbf{k}dk_z/(2\pi)^3$. Excluding $\psi_{\text{SC}}^{\mathbf{k},k_z,\omega}$, we can rewrite the latter equation as

$$\int_{\mathbf{k}} (\psi_{\text{TI}}^{\mathbf{k},\omega})^\dagger \psi_{\text{TI}}^{\mathbf{k},\omega} + \int_{\mathbf{k}} (\psi_{\text{TI}}^{\mathbf{k},\omega})^\dagger \hat{P}_{\mathbf{k},\omega} \psi_{\text{TI}}^{\mathbf{k},\omega} = 1, \quad \text{where} \quad (17)$$

$$\hat{P}_{\mathbf{k},\omega} = \int_{k_z} T_{\mathbf{k},k_z}^\dagger (\omega - H_{\text{SC}}^{\mathbf{k},k_z})^{-2} T_{\mathbf{k},k_z} = -\frac{\partial \Sigma_{\mathbf{k},\omega}}{\partial \omega}. \quad (18)$$

We will see below that $\psi_{\text{TI}}(\mathbf{r})$ varies over a length scale $\sim \xi$. Consequently, $v|\mathbf{k} - \mathbf{M}| \sim \Delta$. In such a regime, we can assume that $\hat{P}_{\mathbf{k},\omega} \approx \hat{P}_{\mathbf{M},\omega}$. Using Eq. (10), where δU is virtually independent of ω , we obtain

$$\hat{P}_{\mathbf{M},\omega} = \lambda\Delta \frac{\Delta\tau_0 - \omega\tau_x}{(\Delta^2 - \omega^2)^{3/2}}, \quad |\omega| < \Delta. \quad (19)$$

In this approximation \hat{P} is momentum independent, and Eq. (16) can be rewritten in real space as

$$\int d^2\mathbf{r} [\psi_{\text{TI}}^\omega(\mathbf{r})]^\dagger (1 + \hat{P}_{\mathbf{M},\omega}) \psi_{\text{TI}}^\omega(\mathbf{r}) = 1. \quad (20)$$

Observe that for $|\omega|$ approaching $|\Delta|$, the matrix \hat{P} diverges. This divergence occurs because in the regime $0 < |\Delta| - |\omega| \ll |\Delta|$ an electron spends a large portion of its time in the superconductor. Therefore, the norm of $\psi_{\text{SC}} = \hat{P}\psi_{\text{TI}}$ increases relative to the norm of ψ_{TI} .

D. Equations for the effective wave function

We are looking for solutions of the Bogolyubov-de Gennes equations Eq. (11) which correspond to bound states. Consequently, the energies of these solutions ω should be smaller than the proximity-induced gap Δ_{TI} , which satisfies the equation [19],

$$\frac{\Delta_{\text{TI}}}{\lambda} = \sqrt{\frac{\Delta - \Delta_{\text{TI}}}{\Delta + \Delta_{\text{TI}}}}. \quad (21)$$

Imagine now that l vortices end up trapped by the hole. In such a situation, the order parameter $\Delta(\mathbf{r})$ can be expressed as [33]

$$\Delta(\mathbf{r}) = |\Delta(r)|e^{il\theta}, \quad (22)$$

where r and θ are polar coordinates, and $|\Delta(r)| \rightarrow |\Delta|$ when $r \rightarrow \infty$. If the hole radius R is large, $R > \xi$, $|\Delta(r)|$ can be approximated as

$$|\Delta(r)| = |\Delta|\Theta(r - R), \quad (23)$$

where $\Theta(r)$ is the Heaviside step function.

Let us define a spinor F as

$$\psi_{\text{TI}} = \exp[-i\theta(l\tau_z + \sigma_z)/2 + i\mu\theta]F^\mu(r), \quad (24)$$

$$F^\mu = (f_1^\mu, f_2^\mu, f_3^\mu, -f_4^\mu)^T.$$

The physical meaning of μ is the total angular momentum of the state. The transformation in Eq. (24) is well defined only when

$$j = \mu + \frac{l+1}{2} \quad (25)$$

is an integer. In other words, when the number of vortices l is odd (even), the angular momentum μ is integer (half-integer).

Substituting Eqs. (12), (15), and (24) in Eq. (11) we derive

$$\begin{aligned} i\tilde{v}\left(\frac{d}{dr} + \frac{2\mu + l + 1}{2r}\right)f_2^\mu + |\tilde{\Delta}|f_3^\mu - (\omega + \tilde{U})f_1^\mu &= 0, \\ i\tilde{v}\left(\frac{d}{dr} - \frac{2\mu + l - 1}{2r}\right)f_1^\mu - |\tilde{\Delta}|f_4^\mu - (\omega + \tilde{U})f_2^\mu &= 0, \\ i\tilde{v}\left(\frac{d}{dr} + \frac{2\mu - l + 1}{2r}\right)f_4^\mu + |\tilde{\Delta}|f_1^\mu - (\omega - \tilde{U})f_3^\mu &= 0, \\ i\tilde{v}\left(\frac{d}{dr} - \frac{2\mu - l - 1}{2r}\right)f_3^\mu - |\tilde{\Delta}|f_2^\mu - (\omega - \tilde{U})f_4^\mu &= 0. \end{aligned} \quad (26)$$

These equations are the foundation on which the main results of this paper are based. These equations will be solved and analyzed for different values of ω , μ , and l . Since Eq. (26) admits the following symmetry: $\mu \leftrightarrow -\mu$, $f_4 \leftrightarrow if_1$, $f_3 \leftrightarrow if_2$, $\tilde{U} \leftrightarrow -\tilde{U}$, only $\mu \geq 0$ solutions have to be found explicitly.

We mentioned above that, upon contact, the superconductor dopes the surface states of the topological insulator. Consequently, U becomes a function of r . However, we assume below that $U = 0$, since this condition is most favorable for the observation of the Majorana fermion. To satisfy this requirement, an external gate electrode controlling U might be necessary. If $U(r)$ is nonzero, yet remains small for any r , then perturbation theory can be used to account for it.

III. ZERO-ENERGY SOLUTION

In this section, we will obtain all zero-energy ($\omega = 0$) solutions. Such solutions are often called ‘‘zero modes’’. It will be shown that the number of zero modes is equal to the number of vortices in the hole l .

If $\omega = \tilde{U} = 0$, the system of Eq. (26) decouples into two sets of equations,

$$i\tilde{v}\left(\frac{d}{dr} - \frac{2\mu + l - 1}{2r}\right)f_1^\mu - |\tilde{\Delta}|f_4^\mu = 0, \quad (27)$$

$$i\tilde{v}\left(\frac{d}{dr} + \frac{2\mu - l + 1}{2r}\right)f_4^\mu + |\tilde{\Delta}|f_1^\mu = 0,$$

and

$$i\tilde{v}\left(\frac{d}{dr} + \frac{2\mu + l + 1}{2r}\right)f_2^\mu + |\tilde{\Delta}|f_3^\mu = 0, \quad (28)$$

$$i\tilde{v}\left(\frac{d}{dr} - \frac{2\mu - l - 1}{2r}\right)f_3^\mu - |\tilde{\Delta}|f_2^\mu = 0,$$

where $|\tilde{\Delta}| = |\tilde{\Delta}(r)|$ is given by Eq. (23).

Outside the hole ($r > R$), the gap $|\tilde{\Delta}|$ is nonzero. Finite solutions of Eqs. (27) and (28) can be expressed in terms of the modified Bessel functions $K_m(x)$:

$$\begin{aligned} f_1 &= Ar^{\frac{l}{2}}K_{\mu-1/2}\left(\frac{\lambda r}{v}\right), & f_4 &= -iAr^{\frac{l}{2}}K_{\mu+1/2}\left(\frac{\lambda r}{v}\right), \\ f_2 &= Br^{-\frac{l}{2}}K_{\mu+1/2}\left(\frac{\lambda r}{v}\right), & f_3 &= -iBr^{-\frac{l}{2}}K_{\mu-1/2}\left(\frac{\lambda r}{v}\right). \end{aligned} \quad (29)$$

In the hole ($r < R$) we have $\tilde{\Delta} = 0$ and these systems decouple further into four independent equations. They can be easily solved:

$$\begin{aligned} f_1 &= C_1r^{\mu+\frac{l-1}{2}}, & f_4 &= C_4r^{\frac{l-1}{2}-\mu}, \\ f_2 &= C_2r^{-\mu-\frac{l+1}{2}}, & f_3 &= C_3r^{\mu-\frac{l+1}{2}}. \end{aligned} \quad (30)$$

Of these four functions, f_2 has the strongest singularity at $r = 0$. Since a wave function has to be normalizable: $\int r dr |f_2|^2 < \infty$, the divergence of f_2 must not be too strong: $\mu + (l + 1)/2 < 1$. For positive μ and l this inequality cannot be satisfied simultaneously with the condition (25). Therefore, $C_2 = 0$. Further, the function f_4 is normalizable when

$$\mu < \frac{l + 1}{2}. \quad (31)$$

Matching the solutions of Eqs. (30) and (29) at $r = R$, we conclude that $f_2 = f_3 = 0$, while $f_{1,4}$ are nonzero only if Eq. (31) is satisfied.

Using the symmetry between positive and negative μ , one can generalize Eq. (31) for arbitrary μ :

$$|\mu| < \frac{l + 1}{2}. \quad (32)$$

As explained above, the condition that j , Eq. (25), is an integer implies that μ is an integer, if l is odd, and μ is a half-integer, if l is even. Keeping this in mind, one discovers that there are no zero-energy solutions in the absence of the vortex, $l = 0$. There is a single zero mode with $\mu = 0$, if $l = 1$. In the case of two vortices in the hole, $l = 2$, we have two zero-energy solutions with $\mu = \pm 1/2$; if $l = 3$ there exist three zero-energy solutions with $\mu = 0, \pm 1$, etc. One can convince oneself that the number of zero-energy solutions coincides with the number l of vortices in the hole.

This connection between the number of zero modes and l may be detected experimentally: It implies that the zero-bias anomaly of the tunneling spectrum is sensitive to the magnetic field. We will discuss this in more detail in Sec. V.

IV. SYSTEM WITH A SINGLE VORTEX

In this section we study a system with a single vortex pinned by a hole ($l = 1$). Since l is odd, the vortex hosts a single Majorana fermion. This Majorana fermion state can be detected in the tunneling experiment depicted in Fig. 1. It manifests itself as a zero-bias anomaly of the tunneling spectrum. We will determine the parameter range where the zero-bias anomaly current is the strongest.

In addition to the Majorana fermion state, a set of subgap excited states is localized in the core of the vortex (the term ‘‘subgap state’’ implies that the eigenenergy of such a state lies within the bulk single-electron gap: $|\omega| < \Delta_{\text{TI}}$). Unlike a typical Abrikosov vortex, whose core is filled with a dense CdGM spectrum, in our situation the number of subgap states is small: There can be as few as two states with positive eigenenergies (and, respectively, two states with $\omega < 0$). We will numerically calculate the subgap spectrum and discuss the optimization of the system parameters to

facilitate the detection of this spectrum in a tunneling experiment.

A. Majorana fermion

When $l = 1$ the solution for the Majorana fermion, Eqs. (29) and (30) with $\mu = 0$, continuous at $r = R$, reads

$$\begin{aligned} f_1 &= -if_4 = C_1, \quad r < R, \\ f_1 &= -if_4 = C_1 \exp[-\lambda(r - R)/v], \quad r > R, \end{aligned} \quad (33)$$

where C_1 is a constant.

For the tunneling experiment depicted in Fig. 1, it is important that the wave function of a probed state is well localized within the hole. As a measure of such localization, let us calculate the following ratio:

$$I = \frac{\int_R^{+\infty} (1 + \widehat{P}_{M,0}) \rho(r) 2\pi r dr}{\int_0^R \rho(r) 2\pi r dr}, \quad (34)$$

where the probability density $\rho(r)$ is equal to

$$\begin{aligned} \rho(r) &= |f_1(r)|^2 + |f_2(r)|^2 + |f_3(r)|^2 + |f_4(r)|^2 \\ &= 2|C_1|^2 \begin{cases} 1, & r < R, \\ \exp\left[-\frac{2\lambda}{\Delta} \frac{(r-R)}{\xi}\right], & r > R, \end{cases} \end{aligned} \quad (35)$$

and the operator $\widehat{P}_{M,0}$ (accounts for the tunneling into the superconductor) equals to

$$\widehat{P}_{M,0} = \begin{cases} 0, & r < R, \\ \frac{\lambda}{\Delta}, & r > R. \end{cases} \quad (36)$$

Here we use the relation $v = \Delta\xi$. The quantity I varies from 0 to $+\infty$. If $I = 0$, the Majorana fermion is localized entirely within the hole radius; when I is large the wave function spreads out deeply into the bulk. Thus, to enlarge the tunneling current we want to have a small I . Simple calculations show that

$$I = \left(\frac{\xi}{R}\right) \left(1 + \frac{\Delta\xi}{2\lambda R}\right) \left(1 + \frac{\Delta}{\lambda}\right). \quad (37)$$

Since $R > \xi$, to have a small $I < 2$, we need $\lambda/\Delta > 1.7$. Below we will see that this inequality will be satisfied in the optimal regime.

B. Equation for the energies of the excited states

When $\omega \neq 0$, the solution of Eq. (26) in the hole ($r < R$) can be expressed in terms of the Bessel functions $J_\nu(z)$:

$$\begin{aligned} f_1^\mu &= iAJ_\mu\left(\frac{\omega r}{\Delta\xi}\right), \quad f_2^\mu = AJ_{\mu+1}\left(\frac{\omega r}{\Delta\xi}\right), \\ f_3^\mu &= iBJ_{\mu-1}\left(\frac{\omega r}{\Delta\xi}\right), \quad f_4^\mu = BJ_\mu\left(\frac{\omega r}{\Delta\xi}\right). \end{aligned} \quad (38)$$

If $r > R$, it is convenient to introduce the following linear combinations [19]:

$$\begin{aligned} X_1^\mu &= if_1^\mu + f_4^\mu, \quad X_2^\mu = if_1^\mu - f_4^\mu, \\ Y_1^\mu &= if_2^\mu + f_3^\mu, \quad Y_2^\mu = if_2^\mu - f_3^\mu, \end{aligned} \quad (39)$$

$$Y_1^\mu = \frac{i\tilde{v}}{\omega} \left(\frac{dX_1^\mu}{dr} - \frac{1}{\tilde{\xi}} \frac{|\tilde{\Delta}|}{\sqrt{|\tilde{\Delta}|^2 - \omega^2}} X_1^\mu - \frac{\mu}{r} X_2^\mu \right), \quad (40)$$

$$Y_2^\mu = \frac{i\tilde{v}}{\omega} \left(\frac{dX_2^\mu}{dr} + \frac{1}{\tilde{\xi}} \frac{|\tilde{\Delta}|}{\sqrt{|\tilde{\Delta}|^2 - \omega^2}} X_2^\mu - \frac{\mu}{r} X_1^\mu \right), \quad (41)$$

where $\tilde{\xi}(\omega) = \frac{\tilde{v}}{\sqrt{|\tilde{\Delta}|^2 - \omega^2}}$,

and express the solutions in terms of Whittaker functions [34],

$$X_{1,2}^\mu = \frac{C_{1,2}}{\sqrt{r}} W_{\alpha_{1,2},\mu} \left(\frac{2r}{\tilde{\xi}(\omega)} \right), \quad (42)$$

$$\alpha_{1,2} = \mp \frac{|\tilde{\Delta}|}{2\sqrt{|\tilde{\Delta}|^2 - \omega^2}}. \quad (43)$$

Since we seek the subgap solutions ($\omega < |\Delta_{\text{II}}|$), the values $\alpha_{1,2}(\omega)$ and $\tilde{\xi}(\omega)$ are real, and the latter can be considered as a characteristic localization length of the excitation with energy ω . Matching solutions at $r = R$, we derive the following equation for the eigenenergies ω of the subgap excited states,

$$\begin{aligned} &\left(\frac{W'_{\alpha_{1,\mu}}}{\tilde{\xi} W_{\alpha_{1,\mu}}} + \frac{W'_{\alpha_{2,\mu}}}{\tilde{\xi} W_{\alpha_{2,\mu}}} - \frac{\mu + 1/2}{R} + \frac{\omega J_{\mu+1}}{\tilde{v}_\mu J_\mu} \right) \\ &\times \left(\frac{W'_{\alpha_{1,\mu}}}{\tilde{\xi} W_{\alpha_{1,\mu}}} + \frac{W'_{\alpha_{2,\mu}}}{\tilde{\xi} W_{\alpha_{2,\mu}}} + \frac{\mu - 1/2}{R} - \frac{\omega J_{\mu-1}}{\tilde{v}_\mu J_\mu} \right) \\ &= \left(\frac{W'_{\alpha_{1,\mu}}}{\tilde{\xi} W_{\alpha_{1,\mu}}} - \frac{W'_{\alpha_{2,\mu}}}{\tilde{\xi} W_{\alpha_{2,\mu}}} - \frac{\tilde{\Delta}}{\tilde{v}} \right)^2. \end{aligned} \quad (44)$$

Here the Whittaker functions $W_{\alpha,\mu}(z)$ are taken at $z = 2R/\tilde{\xi}(\omega)$ and the Bessel functions $J_\alpha(z)$ at $z = \omega R/v$. Prime means differentiation over z : $W'_{\alpha,\mu}(z) = dW_{\alpha,\mu}(z)/dz$.

Equation (44) corrects a misprint in Eq. (41) of Ref. [19]. There, instead of the valid $(\mu \pm 1/2)/R$ terms, the incorrect $(\mu \pm 1)/R$ are shown.

C. The first and higher excited states

Equation (44) can be used to study the dependence of the eigenenergies of the subgap states on the system parameters R/ξ and λ/Δ . Each excited state can be characterized [19,28] by a pair of quantum numbers μ, n , where n is the principal quantum number of a solution of Eq. (44) with a given μ .

Our numerical analysis shows that the lowest excited state of our system corresponds to the quantum numbers $\mu = 1$ and $n = 0$. The energy of the first excited state, as a function of the hole radius $R > \xi$, is plotted in Fig. 2 for different barrier transparencies λ/Δ . Note that we do not calculate the energy for small values of R . Indeed, if $R < \xi$, the developed formalism becomes invalid and, in addition, in such a regime the Caroli-de Gennes-Matricon levels begin populating the core of the vortex.

As we can see from Fig. 2, the energy gap between the first excitation and the Majorana fermion decreases when R increases. This is quite a natural behavior: The growth of the radius R leads to an increase of the effective confinement area. As it is seen from the results shown in Fig. 2, the hole radius must not exceed several ξ , otherwise, the gap between the Majorana fermion and the excited states shrinks too much.

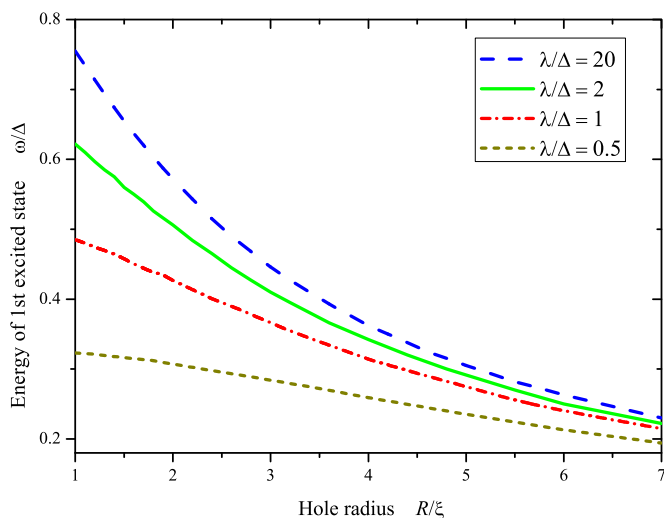


FIG. 2. (Color online) Normalized energy $\frac{\omega}{\Delta}$ of the first excited state ($\mu = 1$ and $n = 0$) as a function of the normalized hole radius R/ξ for different barrier transparencies λ . The energy of the first excited state is bounded from above by $\Delta_{\text{TI}}(\lambda)$ (the gap in the topological insulator), which is a decreasing function of λ . For $\lambda = 20\Delta$, solving Eq. (21), we find that $\Delta_{\text{TI}} \approx \Delta$. When $\lambda = 2\Delta$, the gap $\Delta_{\text{TI}} \approx 0.75\Delta$; when $\lambda = \Delta$, the gap $\Delta_{\text{TI}} \approx 0.54\Delta$. Finally, $\Delta_{\text{TI}}(0.5\Delta) \approx 0.35\Delta$.

It also follows from Fig. 2 that the increased transparency of the barrier between the topological insulator and the superconductor, $\lambda \gg \Delta$, does not give rise to a significant increase of the gap compared with the case $\lambda/\Delta \simeq 2$. If we choose $2 < R/\xi < 4$ and $\lambda \geq 2\Delta$, then the gap is about 0.4–0.6 in units of Δ .

Similar to Eq. (35), we can calculate the probability density $\rho_1(0)$ in the center of the hole for the first excited state. The corresponding wave function is given by Eqs. (29) and (30). These expressions have to be matched at $r = R$. For $r > R$, the normalization condition Eq. (20) must be used. Numerical results show that $\rho_1(0)$ for the chosen range of parameters is of the same order as that for the Majorana fermion $\rho(0)$: $\rho_1(0)/\rho(0) \approx 0.67$. The excitation with the orbital number $-\mu$ has the same energy with the excitation μ . Total density of the states at the center of the hole with the same energy ω_1 would be $2\rho_1(0)$: $2\rho_1(0)/\rho(0) \approx 1.3$. This means that, in an idealized tunneling experiment, both states manifest themselves as peaks of comparable magnitude.

For $R/\xi \lesssim 4.5$ the second excited state has the quantum numbers $\mu = 2, n = 0$ (see Fig. 3). With good accuracy, the energy difference between the first and second excited states is

$$\omega_2 - \omega_1 > 0.1\Delta, \quad (45)$$

when $R/\xi < 4$, and $\lambda > 2\Delta$ (see Fig. 4). However, the probability density at the center of the hole, $\rho_2(0)$, vanishes for this state. Thus, a tunneling experiment, in which the probe is positioned near the center of the hole ($r = 0$), cannot detect this state, unless disorder is present.

The eigenenergies of the lowest-lying excited states are shown in Fig. 3. As one can see from this figure, when R is smaller than some critical value R_{cr} , only two excited states

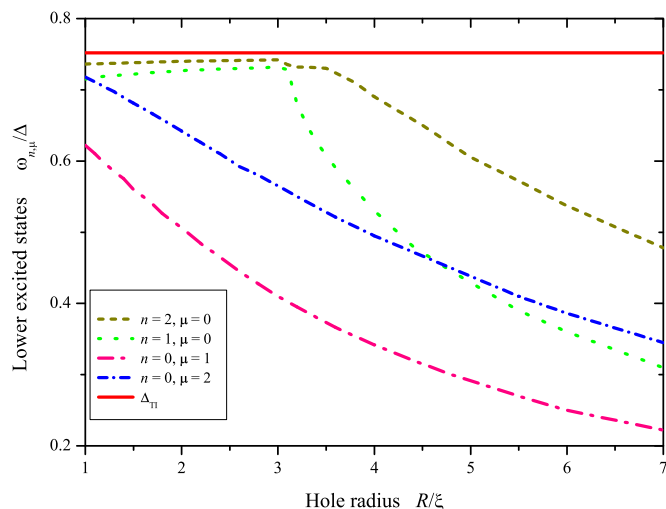


FIG. 3. (Color online) Energy of the low-lying excited states as a function of the normalized hole radius R/ξ for the barrier transparency $\lambda = 2\Delta$. The red horizontal line shows the gap Δ_{TI} , induced in the topological insulator by the proximity effect. Note that the state with $\mu = 2$ has zero probability density at the center of the hole. Thus, it cannot be observed in a tunneling spectrum if the probe is located at $r = 0$. For $R < R_{\text{cr}} \approx 3$, only the state with $\mu = 1, n = 0$, and the Majorana fermion contribute to the spectrum below the gap $|\omega| < \Delta_{\text{TI}}$.

remain. Of these two, only $\mu = 1$ state has finite probability density at $r = 0$. For $R > R_{\text{cr}}$, more states split off from the continuous spectrum and form bound states inside the gap Δ_{TI} .

D. Back-of-the-envelope estimates

The numerical results for the first excited state can be checked against simple “back-of-the-envelope” calculations. A wave function of a subgap state on the surface of the topological insulator is finite for $r < R$, but decays quickly

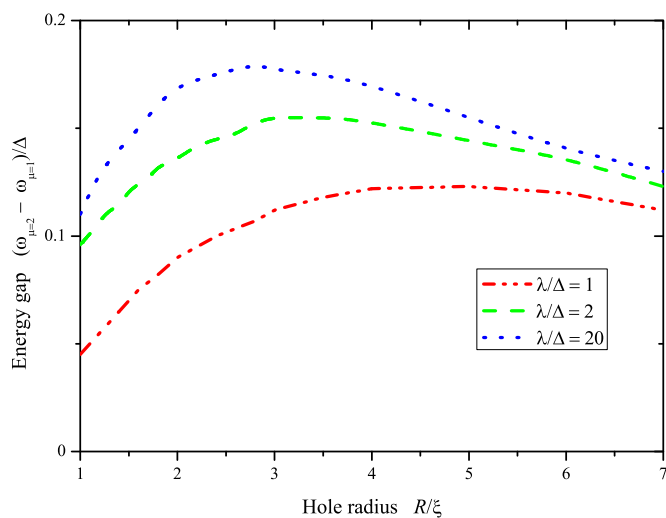


FIG. 4. (Color online) Energy gap between two low-lying excited states, the first excited state ($\mu = 1, n = 0$) and the state $\mu = 2, n = 0$, as a function of the normalized hole radius R/ξ .

for $r - R > \xi$. In other words, because of the superconducting gap, an electron with energy $|\omega_1| < \Delta$ is effectively confined to an area of radius $R_{\text{conf}} = R + \xi$. Therefore, $|\omega_1| \approx v|\mathbf{k}_1|$, where the quantized momentum $|\mathbf{k}_1| \approx \pi/(2R_{\text{conf}})$. This means that

$$\frac{\omega_1}{\Delta} \approx \frac{\pi}{(2R/\xi) + 2} \approx \begin{cases} 0.8 & \text{if } R/\xi = 1.0, \\ 0.2 & \text{if } R/\xi = 7.0. \end{cases} \quad (46)$$

These numbers agree well with the numerical data for large barrier transparencies (see Fig. 2). The quality of this estimate deteriorates for smaller λ , because in this regime the induced gap decreases, and the confinement of the subgap state becomes weaker. As a result, our simple estimate for R_{conf} becomes inaccurate, at least for small R (for larger R the accuracy of this estimate improves, since the hole radius becomes the dominant contribution to R_{conf}).

E. Resolving excited states

In this section we will discuss the optimization of our system for the purpose of resolving the excited states. We will assume that the STS tip is placed above the center of the hole. In such a situation, only states with $\rho(0) > 0$ contribute to the tunnel current. As can be seen from Eq. (39), only states with $\mu = 0, \pm 1$ have a nonzero probability density at the center of the hole. The numerical analysis of Eq. (44) shows that, when $|\mu| \leq 1$, the lowest excited state corresponds to the quantum numbers $n = 0, \mu = 1$, next is the state $n = 1, \mu = 0$, and afterward $n = 2, \mu = 0$.

When $R < R_{\text{cr}}$, of these three states only the state with $n = 0, \mu = 1$ remains inside the gap. Two others are virtually merged with the continuum spectrum above Δ_{TI} .

A hole with a radius of the order of R_{cr} is optimal for the observation of the first excited state. Indeed, in this regime only the first excited state contributes to the tunneling current at the center of the hole. Furthermore, for a broad range of transparencies λ , this state lies close to the middle of the gap $\omega_1 \approx \Delta_{\text{TI}}/2$, being well separated from both the Majorana state at $\omega = 0$ and from the continuum at $|\omega| = \Delta_{\text{TI}}$.

The dependence of R_{cr} on the barrier transparency λ is shown in Fig. 5. The optimal transparency of the barrier $\lambda \geq 2\Delta$, thus, the optimal radius is $2\xi < R < 3\xi$. For these parameters, the gap between the Majorana fermion and the first excited state is about 0.4Δ , and between the first excited state and the continuum is about 0.3Δ .

V. DISCUSSION

Current interest in Majorana fermions is fueled, among other reasons, by the possibility to devise a future topological quantum computer. To realize this Majorana fermion-based computer, Majorana fermion localized states must be created and moved in space in a controllable manner. At present, this appears to be a very distant goal. The more modest objective of creating an immobile Majorana fermion is being pursued now, and certain initial steps are happening in this direction [17,18]. However, no decisive proof of Majorana fermion states is available. In this paper we study a simple heterostructure [19] where an immobile Majorana fermion can be generated. Despite its relative simplicity, the proposed system has several

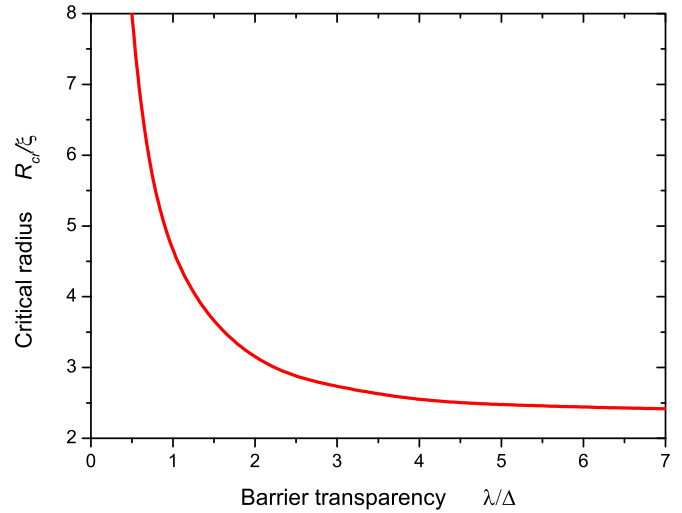


FIG. 5. (Color online) Critical radius R_{cr} as a function of the normalized transparency λ/Δ of the barrier. The critical radius is defined by the requirement that for $R < R_{\text{cr}}$ only one subgap state (see Fig. 3) has nonzero density of states at the center of the hole.

advantages, which can be useful for the experimental detection of the Majorana state. In this section we offer a nontechnical summary of the system's most important features.

A. Large minigap

One of the key characteristics of our system is the substantial energy gap between the zero-energy Majorana fermion and the lowest excited state. This is important since it alleviates requirements on the temperature and the energy resolution of the experiment. By choosing the system parameters adequately, the energy of the first excited state can be as large as $0.4\Delta \sim 4$ K. This gap is much larger than the minigap for CdGM states $\delta\varepsilon \sim \Delta^2/E_{\text{F}} \sim 10^{-2}$ K (we assume that $E_{\text{F}} \sim 10^4$ K and $\Delta \sim 10$ K).

To understand the origin of such a large minigap in our system we can resort to a simple “particle-in-a-box” estimate: A massless Dirac fermion with energy $\omega < \Delta_{\text{TI}}$ is trapped inside a disk of radius $R \sim \xi$ (the entrapment occurs because the particle energy is below the gap Δ_{TI} , thus, it cannot propagate in an environment with a gap, which exists for $r > R$). This simple estimate reproduces the numerical results quite accurately; see Eq. (46). Analyzing the derivation of Eq. (46), one concludes that the large minigap is a consequence of the linear spectrum of the excitations on the surface of the topological insulator.

Finally, we would like to cite Ref. [36], which studied similar heterostructures in the limit of the weak proximity effect $\lambda \ll \Delta$ (we did not study this regime, since it corresponds to a very low induced gap: $\Delta_{\text{TI}} \ll \Delta$). These papers established that the minigap is of the order of the proximity-induced gap. How can these results be applied to our case where $\lambda \sim \Delta$? Note that for very weak λ the minigap is an increasing function of λ . When λ becomes comparable to Δ , the minigap reaches some finite value Δ^* . How does this value compare against Δ ? We notice that in the regime $\lambda \sim \Delta_{\text{TI}} \sim \Delta$ there is only one energy scale in our system, and we conclude that $\Delta^* \sim \Delta$.

The system with such a large minigap deserves a detailed study. Here our aim was twofold: to investigate how the local tunneling spectroscopy can be used to prove the existence of the Majorana fermion in our setup (Sec. VB), and to optimize the parameters of the system for such an experiment (Sec. VC).

B. Tunneling spectroscopy of the core

The Majorana fermion should manifest itself on a tunneling experiment as a zero-bias peak. However, the zero-bias peak may be caused by other mechanisms (see, for example, the analysis of Ref. [35]), thus, additional verifications are necessary. In this paper we discussed two types of further measurements. First, one can study the dependence of the zero-bias anomaly on the magnetic field. As it follows from Eq. (32), the number of zero modes is equal to the vorticity pinned by the hole. Thus, when the field is increased, in the disorder-free system the strength of the zero-bias anomaly should experience a stepwise increase each time an extra flux quantum enters the pinning hole. If disorder is present, the behavior of the zero-bias anomaly changes. The disorder potential lifts the degeneracy of the zero-energy states (splitting of the zero-energy manifold by a perturbation is studied in Ref. [38]). However, due to symmetry [see Eq. (7)], the parity of the zero-mode number remains unchanged by the disorder. Therefore, for even (odd) vorticity l there is no (single) zero-energy Majorana fermion state bound to the hole. This means that, if weak disorder is present, the zero-bias anomaly demonstrates a nonmonotonous dependence on the magnetic field. The experimental verification of such a nonmonotonicity would be a strong argument in favor of Majorana fermion states in our heterostructure. Of course, inducing multiply quantized vortex in experiment is a complicated, but not insurmountable, issue [37].

Magnetic field may also lift the degeneracy of the zero-energy states. We already explained above that the magnetic field significantly affects a particular state only when the flux through the area where this state is localized is comparable with the flux quantum. In our situation, this condition is not satisfied, and it is possible to apply perturbation theory in orders of the vector-potential \mathbf{A} to account for the magnetic field. Equations (29) and (30) for the zero-energy wave functions valid for $U = 0$ can be used to evaluate the corresponding matrix elements. However, it is easy to check that these matrix elements are identically zero. They may become finite only when $U \neq 0$. Consequently, in the limit $|U| \ll \Delta$, which is the most suitable for observation of the Majorana fermion, the splitting due to the magnetic field is very weak, at least when the trapped vorticity remains small. When the vorticity grows, a more advanced treatment might be required. However, at large vorticity the detrimental effects of magnetic field on the superconducting structure degrade the performance of the system in a variety of ways. Thus, the limit of strong magnetic field is outside the optimal regime, and we will not study it in this paper.

The second type of measurements we discussed is the resolution of the excited subgap states bound to the hole. Unlike the classical CdGM states, which densely fill the core of a vortex, only a small number of subgap excitations exists in our setup. Strictly speaking, a successful detection of these excitations does not constitute a proof for Majorana fermion

existence. Yet, it would provide an additional check point validating the theoretical description of the heterostructure.

C. System parameter optimization

To facilitate experiments we investigated the possible optimization of the system parameters. We found that if the tunneling probe is situated over the center of the hole, only excitations with small n and μ contribute to the tunneling conductance. Excited states with higher n and μ are localized closer to the hole periphery; thus, they do not affect significantly such a tunneling spectrum. Consequently, if

$$\frac{R}{\xi} \simeq 2 - 3, \quad \frac{\lambda}{\Delta} \geq 2, \quad (47)$$

then only a single subgap state can be seen in the tunneling spectrum measured at $r = 0$. Under these conditions, the energy gap between the Majorana fermion and this excited state is about 0.4Δ , and between the excited state and the continuum above the superconducting gap is about 0.3Δ . The numerically calculated tunneling conductance for this situation is presented in Fig. 6.

To obtain some estimates, let us now take the characteristic values $T_c = 10$ K and $\Delta = 1.76T_c \approx 17.6$ K for a BCS-type superconductor. Then we obtain the optimal value $\lambda \gtrsim 4$ meV. From Fig. 6 we conclude that $T \lesssim 0.2$ – 0.5 K is needed to resolve the Majorana fermion and the excited states. To find the radius of the hole we use the formula $\xi = v/\Delta \approx 200$ nm (using the value $v = 5.0 \times 10^7$ cm/s reported in Ref. [39] for Bi_2Se_3). Thus, $R \sim 400$ – 600 nm.

During our discussion we tacitly assumed that the coherence length in the superconductor ξ_{SC} is identical to $\xi = v/\Delta$. For BCS superconductor this implies that the Fermi velocity in the superconductor is equal to v . Fortunately, such a restriction may be replaced by a much weaker requirement: $R > \xi_{\text{SC}}$. This

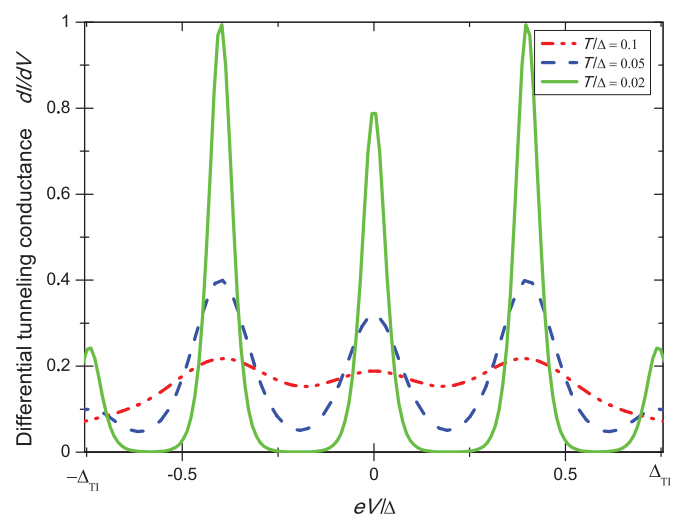


FIG. 6. (Color online) Differential tunneling conductance for different temperatures and optimal values of the parameters $R/\xi = 3$ and $\lambda/\Delta = 2$. Majorana state is responsible for the zero-bias peak. When the STS tip is placed above the center of the hole ($r = 0$), only one excited state ($\mu = \pm 1, n = 0$) contributes to the tunneling spectrum. This state corresponds to peaks at $eV = \pm 0.4\Delta$.

guarantees that the vortex core contains no CdGM states, and our derivation of the effective Hamiltonian is valid.

To conclude, we discuss the application of scanning tunneling spectroscopy to investigate localized states in the topological insulator/superconductor heterostructure presented in Fig. 1. STS can be used to detect the oscillation of the zero-bias anomaly strength when the magnetic field is varied, and to resolve subgap excited states. The successful observation of both phenomena would provide strong evidence in favor of the existence of a Majorana fermion state bound to the hole.

ACKNOWLEDGMENTS

This work was partly supported by the ARO, RIKEN's iTHES program, MURI Center for Dynamic Magneto-Optics, Grant-in-Aid for Scientific Research (S), MEXT Kakenhi on Quantum Cybernetics, the JSPS via its FIRST program, the Russian Foundation for Basic Research (Projects No. 11-02-00708, No. 11-02-00741, No. 12-02-92100-JSPS, and No. 12-02-00339). The authors would like to thank S. V. Zaitsev-Zotov for useful comments.

-
- [1] E. Majorana, *Nuovo Cimento* **14**, 171 (1937).
 [2] F. Wilczek, *Nat. Phys.* **5**, 614 (2009).
 [3] F. Wilczek, *Nature* (London) **486**, 195 (2012).
 [4] S. B. Chung and S. C. Zhang, *Phys. Rev. Lett.* **103**, 235301 (2009).
 [5] G. E. Volovik, *JETP Lett.* **90**, 398 (2009).
 [6] C. Benjamin and J. K. Pachos, *Phys. Rev. B* **81**, 085101 (2010).
 [7] J. Alicea, *Phys. Rev. B* **81**, 125318 (2010).
 [8] Y. E. Kraus, A. Auerbach, H. A. Fertig, and S. H. Simon, *Phys. Rev. Lett.* **101**, 267002 (2008); *Phys. Rev. B* **79**, 134515 (2009).
 [9] S. Fujimoto, *Phys. Rev. B* **77**, 220501 (2008).
 [10] M. Sato and S. Fujimoto, *Phys. Rev. B* **79**, 094504 (2009).
 [11] L. Fu and C. L. Kane, *Phys. Rev. Lett.* **100**, 096407 (2008).
 [12] J. D. Sau, R. M. Lutchyn, S. Tewari, and S. Das Sarma, *Phys. Rev. B* **82**, 094522 (2010).
 [13] M. Sato, Y. Takahashi, and S. Fujimoto, *Phys. Rev. Lett.* **103**, 020401 (2009); *Phys. Rev. B* **82**, 134521 (2010); M. Sato, Y. Takahashi, and S. Fujimoto, M. Sato and S. Fujimoto, *Phys. Rev. Lett.* **105**, 217001 (2010).
 [14] Q.-F. Liang, Z. Wang, and X. Hu, *Europhys. Lett.* **99**, 50004 (2012).
 [15] A. V. Rozhkov, *Int. J. Mod. Phys. B* **12**, 3457 (1998).
 [16] Ch. Nayak, S. H. Simon, A. Stern, M. Freedman, and S. Das Sarma, *Rev. Mod. Phys.* **80**, 3 (2008).
 [17] V. Mourik, K. Zuo, S. M. Frolov, S. R. Plissard, E. P. A. M. Bakkers, and L. P. Kouwenhoven, *Science* **336**, 1003 (2012).
 [18] J. R. Williams, A. J. Bestwick, P. Gallagher, S. S. Hong, Y. Cui, A. S. Bleich, J. G. Analytis, I. R. Fisher, and D. Goldhaber-Gordon, *Phys. Rev. Lett.* **109**, 056803 (2012).
 [19] A. L. Rakhmanov, A. V. Rozhkov, and F. Nori, *Phys. Rev. B* **84**, 075141 (2011).
 [20] P. A. Ioselevich and M. V. Feigel'man, *Phys. Rev. Lett.* **106**, 077003 (2011).
 [21] P. A. Ioselevich, P. M. Ostrovsky, and M. V. Feigel'man, *Phys. Rev. B* **86**, 035441 (2012).
 [22] P. Zareapour, A. Hayat, S. Y. F. Zhao, M. Kreshchuk, A. Jain, D. C. Kwok, N. Lee, S.-W. Cheong, Z. Xu, A. Yang, G. Gu, S. Jia, R. J. Cava, and K. S. Burch, *Nat. Commun.* **3**, 1056 (2012).
 [23] B. Sacépé, J. B. Oostinga, J. Li, A. Ubalini, N. J. Couto, E. Giannini, and A. F. Morpurgo, *Nat. Commun.* **2**, 575 (2011).
 [24] M. Veldhorst, M. Snelder, M. Hoek, T. Gang, V. K. Guduru, X. L. Wang, U. Zeitler, W. G. van der Wiel, A. A. Golubov, H. Hilgenkamp, and A. Brinkman, *Nat. Mater.* **11**, 417 (2012).
 [25] M.-X. Wang, C. Liu, J.-P. Xu, F. Yang, L. Miao, M.-Y. Yao, C. L. Gao, C. Shen, X. Ma, X. Chen, Z.-A. Xu, Y. Liu, S.-C. Zhang, D. Qian, J.-F. Jia, and Q.-K. Xue, *Science* **336**, 52 (2012).
 [26] M. Z. Hasan and C. L. Kane, *Rev. Mod. Phys.* **82**, 3045 (2010).
 [27] D. A. Ivanov, *Phys. Rev. Lett.* **86**, 268 (2001).
 [28] C. Caroli, P. G. de Gennes, and J. Matricon, *Phys. Lett.* **9**, 307 (1964); R. G. Mints and A. L. Rakhmanov, *Solid State Commun.* **16**, 747 (1975).
 [29] A. S. Mel'nikov, A. V. Samokhvalov, and M. N. Zubarev, *Phys. Rev. B* **79**, 134529 (2009).
 [30] A. F. Volkov, P. H. C. Magnée, B. J. van Wees, and T. M. Klapwijk, *Physica C* **242**, 261 (1995).
 [31] N. B. Kopnin and A. S. Melnikov, *Phys. Rev. B* **84**, 064524 (2011).
 [32] N. B. Kopnin, I. M. Khaymovich, and A. S. Mel'nikov, *Phys. Rev. Lett.* **110**, 027003 (2013).
 [33] G. E. Blonder, M. Tinkham, and T. M. Klapwijk, *Phys. Rev. B* **25**, 4515 (1982).
 [34] NIST Digital Library of Mathematical Functions, <http://dlmf.nist.gov/13>.
 [35] J. Liu, A. C. Potter, K. T. Law, and P. A. Lee, *Phys. Rev. Lett.* **109**, 267002 (2012).
 [36] B. Seradjeh, *Nucl. Phys. B* **805**, 182 (2008); I. M. Khaymovich, N. B. Kopnin, A. S. Melnikov, and I. A. Shereshevskii, *Phys. Rev. B* **79**, 224506 (2009).
 [37] T. Cren, L. Serrier-Garcia, F. Debontridder, and D. Roditchev, *Phys. Rev. Lett.* **107**, 097202 (2011).
 [38] M. Cheng, R. M. Lutchyn, V. Galitski, and S. Das Sarma, *Phys. Rev. B* **82**, 094504 (2010).
 [39] H. Zhang, C.-X. Liu, X.-L. Qi, X. Dai, Zh. Fang, and S.-C. Zhang, *Nat. Phys.* **5**, 438 (2009).